

SCoCCA: Multi-modal Sparse Concept Decomposition via Canonical Correlation Analysis

Ehud Gordon* Meir Yossef Levi* Guy Gilboa
 Viterbi Faculty of Electrical and Computer Engineering
 Technion – Israel Institute of Technology, Haifa, Israel

{ehud.gordon,me.levi}@campus.technion.ac.il; guy.gilboa@ee.technion.ac.il

Abstract

Interpreting the internal reasoning of vision-language models is essential for deploying AI in safety-critical domains. Concept-based explainability provides a human-aligned lens by representing a model’s behavior through semantically meaningful components. However, existing methods are largely restricted to images and overlook the cross-modal interactions. Text–image embeddings, such as those produced by CLIP, suffer from a modality gap, where visual and textual features follow distinct distributions, limiting interpretability. Canonical Correlation Analysis (CCA) offers a principled way to align features from different distributions, but has not been leveraged for multi-modal concept-level analysis. We show that the objectives of CCA and InfoNCE are closely related, such that optimizing CCA implicitly optimizes InfoNCE, providing a simple, training-free mechanism to enhance cross-modal alignment without affecting the pre-trained InfoNCE objective. Motivated by this observation, we couple concept-based explainability with CCA, introducing Concept CCA (CoCCA), a framework that aligns cross-modal embeddings while enabling interpretable concept decomposition. We further extend it and propose Sparse Concept CCA (SCoCCA), which enforces sparsity to produce more disentangled and discriminative concepts, facilitating improved activation, ablation, and semantic manipulation. Our approach generalizes concept-based explanations to multi-modal embeddings and achieves state-of-the-art performance in concept discovery, evidenced by reconstruction and manipulation tasks such as concept ablation.

1. Introduction

Developing transparent and trustworthy neural networks remains a major challenge for deploying learning systems, particularly in safety-critical domains such as autonomous

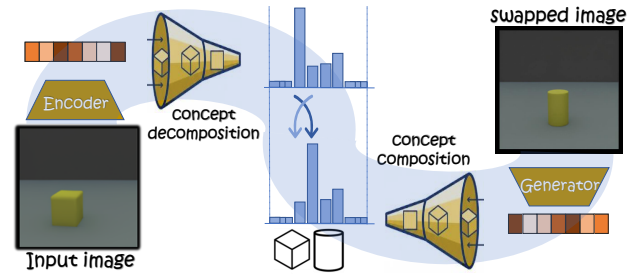


Figure 1. **Concept Swapping.** Beyond explainability, concept decomposition enables controllable manipulation. Using SCoCCA, an embedding can be decomposed into interpretable concepts (e.g., cube and cylinder), their magnitudes swapped, and the modified embedding recomposed to synthesize an image reflecting the swapped concepts.

driving [57] and medical decision-making [1]. Concept-based explainability (C-XAI) offers an interpretable framework for analyzing deep representations through human-understandable units, termed *concepts*. Rather than relying on pixel-level saliency or feature attribution, C-XAI decomposes internal activations into disentangled, semantically coherent components that align naturally with human perception. As modern learning systems increasingly integrate multiple modalities, analyzing how multimodal learning organizes and shares conceptual structure becomes imperative. However, existing efforts have largely focused on the visual domain, leaving open the question of how concept-based explanations can be extended to multimodal networks that jointly learn from text, images, and beyond.

C-XAI has been extensively explored through approaches such as Concept Bottleneck Models [24] and their extensions [7, 22, 56], as well as Concept Activation Vectors [21] and their numerous variants [36, 40, 59]. These approaches, along with more recent formulations such as Varimax [60], remain confined to the image domain and fail to generalize to multi-modal settings, thereby overlooking valuable cross-modal information. More recently, sev-

*Equal contribution.

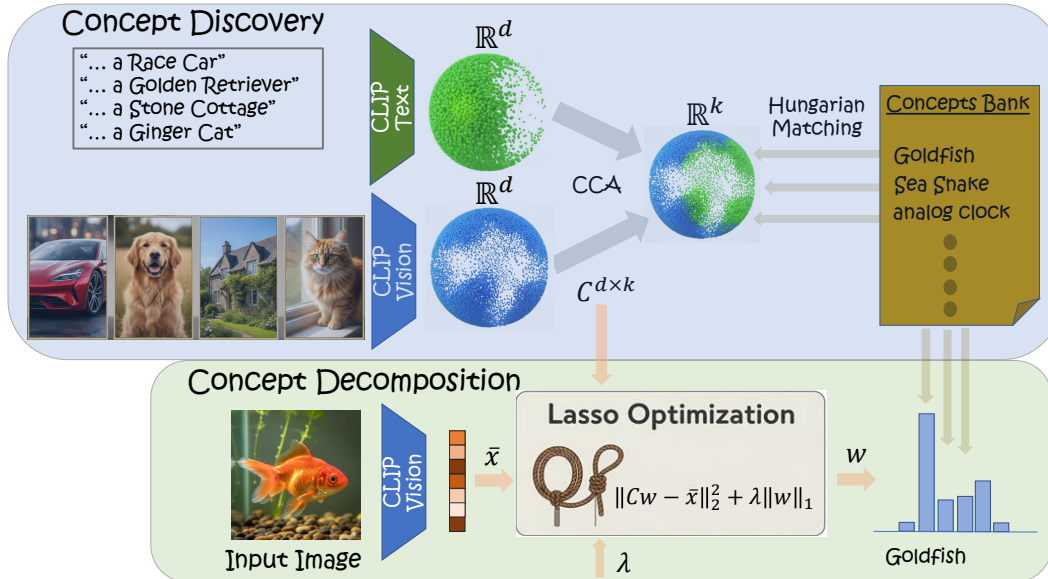


Figure 2. **Method Overview.** In the *Concept Discovery* phase, text and image embeddings are aligned via Canonical Correlation Analysis (CCA) to form a shared latent space. The Hungarian algorithm establishes a one-to-one correspondence between each concept vector and its most relevant item in the concept bank. In the *Concept Decomposition* phase, new embedding is decomposed into concepts by solving a Lasso optimization using the matrix C and the discovered associations.

eral efforts have adapted Sparse Autoencoders (SAEs) to enhance the interpretability of vision and vision–language models (VLMs) [11, 18, 31, 48]. Together with SpLiCE [5], these works advanced concept decomposition in joint text–image embeddings, showing promising results. However, all existing methods either rely solely on the visual modality or overlook the inherent *modality gap* [30] present in CLIP-like architectures. CLIP representations are known to exhibit a modality gap, where image and text features follow distinct distributions with mismatched geometric and probabilistic structures [4, 28], ultimately constraining both interpretability and concept reconstruction quality.

An orthogonal line of research builds on *Canonical Correlation Analysis (CCA)* [15], a well-grounded mathematical framework for aligning distinct observations. These CCA-based approaches, like multi-modal latent alignment schemes [13, 50, 55], emphasize correlation maximization between modalities rather than interpretability or concept analysis. While effective for cross-modal alignment, they overlook the goal of concept-level decomposition. In this work, we show that the CCA and InfoNCE [37] objectives are closely related: optimizing CCA correlates with optimizing the alignment component of the InfoNCE loss, making it a natural choice for aligning networks pre-trained with InfoNCE, such as CLIP [41].

Motivated by this, we propose a method termed *Concept CCA (CoCCA)*, a framework that unifies the interpretability objective of concept-based explainability with the statistical alignment power of CCA. Furthermore, to enhance concept

separation and interpretability, we integrate sparsity principles inspired by C-XAI into the CCA formulation, proposing *Sparse Concept CCA (SCoCCA)*, yielding enhancement in concept decomposition. This sparse variant provides a more sharp and discriminative concept basis, enabling better concept activation, ablation, and swapping as demonstrated in Tab. 1. Our contributions are threefold:

- We extend C-XAI to shared text–image embeddings, providing a unified framework that generalizes naturally to future multimodal foundation models.
- We establish a novel analytical link between CCA and the InfoNCE alignment loss, providing a training-free mechanism enables robust cross-modal concept decomposition.
- We introduce SCoCCA (Sparse CoCCA), a novel framework that enforces an explicit sparsity constraint on the concept decomposition. This mechanism achieves superior concept disentanglement, leading to state-of-the-art efficiency in concept ablation and editing tasks

2. Related Work

Vision-only concept decomposition. The *Concept Activation Vector (CAV)* framework introduced by TCAV [21] defines directional vectors corresponding to human concepts. Extensions such as ACE [12], ICE [59], and CRAFT [10] automate concept discovery by clustering or factorizing activations into coherent groups, building reusable concept banks. In parallel, *Concept Bottleneck*

Models (CBMs) [23] make concepts explicit via an intermediate concept prediction layer, with variants incorporating interactive feedback or memory [7, 47], probabilistic formulations [52], unsupervised or weakly supervised discovery [43, 46], and adaptation to large language models [49]. Another line of research focuses on inducing interpretable structure through low-rank projections and rotations such as PCA, SVD, and Varimax [19, 60], which reveal compact, concentrated axes for human labeling. While these approaches improve interpretability within a single modality, they all overlook the rich mutual information integrated in the multi-modality framework.

Multimodal concept decomposition. Recent work investigates the emergence and alignment of human-interpretable concept axes in vision–language embedding spaces. Methods such as SpLiCE [5] decompose CLIP vision embeddings into sparse additive mixtures of textual concepts, enabling compositional explanations. Complementary studies examine concept discovery directly in pre-trained vision–language models: Zang et al. [58] show that VLMs learn generic visual attributes via their image–text interface, Li et al. [29] evaluate cross-modal alignment of these concepts, and Lee et al. [27] propose language-informed disentangled concept encoders. Parallel approaches from multiview representation learning, such as Canonical Correlation Analysis (CCA) [14], deep CCA [2], and sparse CCA [54], learn shared subspaces across modalities. A notable issue in vision–language models is the modality gap [30], where embeddings from different modalities are spanned in disjoint, non-isotropic distributions, with distinct properties [4, 28, 44]. While current dedicated multimodal concept decomposition methods improve cross-modal understanding, they typically neglect this non-alignment. To our knowledge, our method is the first to explicitly align modalities to better extract mutual cross-modal information.

3. Method

3.1. Concept Decomposition Framework

Notation. We follow the dictionary-learning framework for concept-based decomposition presented by Fel et al. [9]. An encoder f maps images to activations $\mathbf{x} \in \mathbb{R}^d$. For a set of n image inputs, we denote $\mathbf{X} \in \mathbb{R}^{n \times d}$. Similarly, for n text inputs, we denote the activations by $\mathbf{Y} \in \mathbb{R}^{n \times d}$. From these activations we extract a set of k Concept Activation Vectors [21] (CAVs), for each modality. Each CAV is denoted \mathbf{c}_i , and $\mathbf{C} = (\mathbf{c}_1, \dots, \mathbf{c}_k) \in \mathbb{R}^{d \times k}$ forms the concept dictionary. We will focus on computing concept dictionary for the image activations.

We assume a linear relationship between \mathbf{C} and \mathbf{X} , therefore, we look for a coefficient matrix $\mathbf{W} \in \mathbb{R}^{k \times n}$ and a

concept dictionary \mathbf{C} s.t. $\mathbf{X}^\top \approx \mathbf{C}\mathbf{W}$. A desirable concept decomposition should satisfy the following properties:

1. **Reconstruction:** The concept dictionary \mathbf{C} and weights \mathbf{W} should be able to estimate well the original embeddings, i.e., we would like a low value of

$$\ell(\mathbf{C}, \mathbf{W}) = \|\mathbf{C}\mathbf{W} - \mathbf{X}^\top\|_F^2, \quad (1)$$

where $\|\cdot\|_F$ denotes the Frobenius norm.

2. **Sparsity:** The concept coefficients should be sparse, promoting disentangled representations [34], with the objective:

$$\min_{\mathbf{w}} \|\mathbf{w}\|_0, \quad (2)$$

for each coefficient vector \mathbf{w} .

3. **Purity:** Each concept direction \mathbf{c}_i should align with human-understandable semantics. This property is quantitatively assessed by applying concept-ablation and concept-swapping, and evaluating the performance of a linear probe. See Tab. 1.

3.2. Motivation

Despite CLIP being explicitly trained to align positive image–text pairs, it has been observed that its latent space exhibits a *modality gap* [30], where image and text embeddings are linearly separable [28, 44]. To better capture the shared information between modalities, it is desirable to further enhance their alignment. This raises a natural question: *why is applying CCA sensible in the context of CLIP, which is already trained using the InfoNCE loss?* In the following, we elaborate on the relationship between CCA and InfoNCE, demonstrating that the two objectives are closely related.

CCA as whitened alignment. Canonical correlation analysis (CCA) seeks pairs of linear projections of \mathbf{X} and \mathbf{Y} that are *maximally* correlated while remaining mutually orthogonal. In particular, the CCA objective is to find projection matrices $\mathbf{U}, \mathbf{V} \in \mathbb{R}^{d \times d'}$ such that

$$\max_{\mathbf{U}, \mathbf{V}} \text{tr}[(\mathbf{X}\mathbf{U})^\top(\mathbf{Y}\mathbf{V})] \quad (3)$$

subject to

$$(\mathbf{X}\mathbf{U})^\top(\mathbf{X}\mathbf{U}) = \mathbf{I}_{d'}, \quad (\mathbf{Y}\mathbf{V})^\top(\mathbf{Y}\mathbf{V}) = \mathbf{I}_{d'}. \quad (4)$$

Whitening. Let the whitened embeddings be

$$\tilde{\mathbf{X}} := (\mathbf{X} - \mathbf{1}\mu_X^\top)\mathbf{W}_X, \quad \tilde{\mathbf{Y}} := (\mathbf{Y} - \mathbf{1}\mu_Y^\top)\mathbf{W}_Y, \quad (5)$$

with $\mu_X = \frac{1}{n}\mathbf{X}^\top\mathbf{1}$ and $\mu_Y = \frac{1}{n}\mathbf{Y}^\top\mathbf{1}$. The whitening matrix [20] of a set of vectors \mathbf{X} is the linear transformation \mathbf{W}_X satisfying

$$\frac{1}{n}\tilde{\mathbf{X}}^\top\tilde{\mathbf{X}} = \mathbf{I}_d, \quad (6)$$

i.e., a matrix that projects \mathbf{X} to have identity covariance and zero mean. Note that $\mathbf{W}_\mathbf{X}$ is not uniquely determined by (6); in fact, any multiplication of a whitening matrix \mathbf{W} by an orthogonal matrix yields another whitening matrix. A common solution is to choose PCA-whitening. Following Jendoubi and Strimmer [17], we set $\mathbf{W}_\mathbf{X} = \mathbf{U}$, $\mathbf{W}_\mathbf{Y} = \mathbf{V}$. Since \mathbf{U} and \mathbf{V} satisfy Eq. (4), they also satisfy the whitening condition (6). This recasts the CCA objective as a simultaneous whitening of both \mathbf{X} and \mathbf{Y} , which can be rewritten as

$$\max_{\mathbf{U}, \mathbf{V}} \text{tr} [\tilde{\mathbf{X}}^\top \tilde{\mathbf{Y}}]. \quad (7)$$

In other words, CCA can be interpreted as maximizing the alignment between two *whitened* sets of observations.

InfoNCE on whitened inputs. The InfoNCE loss (considering one of the two symmetric directions) can be decomposed into alignment and uniformity terms [53] and written as

$$\mathcal{L}_{\mathbf{X} \rightarrow \mathbf{Y}} = \underbrace{-\frac{1}{N\tau} \text{tr}(\mathbf{X}^\top \mathbf{Y})}_{\text{alignment}} + \underbrace{\frac{1}{N\tau} \mathbf{1}^\top \log(\exp(\mathbf{X}^\top \mathbf{Y}) \mathbf{1})}_{\text{uniformity}}, \quad (8)$$

where $\exp(\cdot)$ and $\log(\cdot)$ are applied element-wise. Then, the InfoNCE loss on whitened embeddings becomes

$$\mathcal{L}_{\tilde{\mathbf{X}} \rightarrow \tilde{\mathbf{Y}}}^{(w)} = \underbrace{-\frac{1}{N\tau} \text{tr}(\tilde{\mathbf{X}}^\top \tilde{\mathbf{Y}})}_{\text{alignment}} + \underbrace{\frac{1}{N\tau} \mathbf{1}^\top \log(\exp(\tilde{\mathbf{X}}^\top \tilde{\mathbf{Y}}) \mathbf{1})}_{\text{uniformity}}. \quad (9)$$

Hence, the alignment term of $\mathcal{L}^{(w)}$ is proportional to the CCA objective (Eq. (7)).

CCA enhances InfoNCE alignment. The above derivation highlights a key insight: maximizing the CCA objective implicitly optimizes the alignment InfoNCE term of whitened inputs. In other words, CCA can *implicitly* enhance the optimization of a pretrained InfoNCE-based model and may be viewed as a fine-tuning strategy. Moreover, CCA offers this benefit with an analytical *closed-form* solution, avoiding the overhead and potential pitfalls of additional training phases.

3.3. Sparse Concept CCA (SCoCCA)

The proposed method consists of two main phases. The first, the *concept discovery* phase, constructs a set of interpretable Concept Activation Vectors (CAVs) organized in the matrix \mathbf{C} , derived from paired image–text embeddings (\mathbf{X}, \mathbf{Y}) . Each CAV is associated with a human-understandable interpretation, and this phase is performed once, a priori. The second, the *concept decomposition* phase, interprets a new, unseen image embedding by leveraging the learned dictionary \mathbf{C} from the fitting phase to decompose its activation into a sparse combination of inter-

pretable concepts, solved via the Lasso optimization procedure [51]. Beyond interpretability, the process is inherently invertible, enabling, for example, selective modification of concept activations, re-composition, and image synthesis through unCLIP [42], as illustrated in Fig. 1. In the following, we elaborate on each of these two phases, which are jointly summarized in Alg. 1.

3.4. Concept Discovery

3.4.1. Concept CCA (CoCCA)

To uncover shared semantic structure across modalities, we extend canonical correlation analysis (CCA) into a concept decomposition framework. CoCCA learns projection matrices specifically projecting to dimension k , $\mathbf{U}, \mathbf{V} \in \mathbb{R}^{d \times k}$ that maximize the correlation between the projected embeddings, as defined by the CCA objective in Eq. (3), subject to the orthogonality constraints in Eq. (4). The resulting projections \mathbf{U} and \mathbf{V} capture directions that are maximally aligned between the image and text embedding spaces. Importantly, this optimization admits a closed-form analytical solution:

$$\mathbf{U} = \Sigma_{\mathbf{X}}^{-1/2} \mathbf{Q}_x, \quad \mathbf{V} = \Sigma_{\mathbf{Y}}^{-1/2} \mathbf{Q}_y, \quad (10)$$

where $\mathbf{Q}_x, \mathbf{Q}_y$ are obtained via the singular value decomposition (SVD) of $\mathbf{M} := \Sigma_{\mathbf{X}}^{-1/2} \Sigma_{\mathbf{X}\mathbf{Y}} \Sigma_{\mathbf{Y}}^{-1/2}$, yielding $\mathbf{M} = \mathbf{Q}_x \mathbf{S} \mathbf{Q}_y^\top$. Here, $\Sigma_{\mathbf{X}}$ and $\Sigma_{\mathbf{Y}}$ denote the covariance matrices of the centered CLIP image and text embeddings, respectively. A detailed derivation of this formulation is provided in the Supp. Finally, the concept bank is constructed from the image projections as:

$$\mathbf{C} := \Sigma_{\mathbf{X}} \mathbf{U}. \quad (11)$$

3.4.2. Concept Matching via the Hungarian Method

Obtaining \mathbf{C} provides a decomposition of the embedding space into concept directions; however, these directions are not yet semantically grounded. In the following, we describe how each direction in \mathbf{C} is associated with a meaningful concept label (e.g., “dog,” “cat,” etc.). Let $\mathbf{C} = [\mathbf{c}_1, \dots, \mathbf{c}_k] \in \mathbb{R}^{d \times k}$ be the learned concept vectors, and let $\{\bar{\mathbf{x}}_i\}_{i=1}^N \subset \mathbb{R}^d$ be the centered CLIP image embeddings for a labeled dataset with M classes and labels $y_i \in \{1, \dots, M\}$. For each class $j \in \{1, \dots, M\}$, we define the index set

$$\mathcal{I}_j = \{i \in \{1, \dots, N\} : y_i = j\},$$

and compute the mean image embedding of that class:

$$\mathbf{p}_j = \frac{1}{|\mathcal{I}_j|} \sum_{i \in \mathcal{I}_j} \bar{\mathbf{x}}_i, \quad j = 1, \dots, M. \quad (12)$$

We then stack these class prototypes into a matrix $\mathbf{P} = [\mathbf{p}_1, \dots, \mathbf{p}_M] \in \mathbb{R}^{d \times M}$. Next, we compute the cosine similarity matrix between concepts and class means:

$$\mathbf{S} = \mathbf{C}^\top \mathbf{P}, \quad S_{ij} = \frac{\langle \mathbf{c}_i, \mathbf{p}_j \rangle}{\|\mathbf{c}_i\|_2 \|\mathbf{p}_j\|_2}. \quad (13)$$

The optimal one-to-one assignment between concepts and classes is obtained by maximizing the total similarity

$$\max_{\mathbf{B}} \sum_{i=1}^k \sum_{j=1}^M S_{ij} B_{ij}, \quad (14)$$

where $\mathbf{B} \in \{0, 1\}^{k \times M}$ is a binary assignment matrix whose rows and columns each contain exactly one nonzero entry, ensuring a unique match between concepts and classes. This assignment is computed efficiently using the Hungarian algorithm [25].

3.4.3. Adding sparsity to CoCCA

With the concept dictionary in hand, we proceed to analyze new, unseen image example. In order to have interpretable, disentangled representation in concept-space, we encourage its weights \mathbf{w} to be sparse. Given new centered image embedding $\bar{\mathbf{x}} \in \mathbb{R}^d$ and a dictionary $\mathbf{C} \in \mathbb{R}^{d \times k}$, we estimate coefficients $\mathbf{w} \in \mathbb{R}^k$ by Lasso [51]:

$$\min_{\mathbf{w} \in \mathbb{R}^k} F(\mathbf{w}) := \underbrace{\frac{1}{2} \|\mathbf{C}\mathbf{w} - \bar{\mathbf{x}}\|_2^2}_{\text{CoCCA}} + \underbrace{\lambda \|\mathbf{w}\|_1}_{\text{Sparsity}}, \quad (15)$$

with $\lambda > 0$, balancing the amount of desired sparsity with reconstruction error. We use the Iterative Shrinkage-Thresholding Algorithm (ISTA) [3], a proximal-gradient method for composite convex problems. ISTA alternates two explicit steps with step size γ at step k :

$$\begin{aligned} \text{(gradient step)} \quad & \mathbf{y}^{(k)} \leftarrow \mathbf{w}^{(k)} - \gamma \mathbf{C}^\top (\mathbf{C}\mathbf{w}^{(k)} - \bar{\mathbf{x}}), \\ \text{(proximal step)} \quad & \mathbf{w}^{(k+1)} \leftarrow S_{\tau\lambda}(\mathbf{y}^{(k)}), \end{aligned} \quad (16)$$

where S_τ is the soft-threshold operator applied component-wise:

$$(S_\tau(\mathbf{y}))_i = \text{sign}(y_i) \max\{|y_i| - \tau, 0\}. \quad (17)$$

We set $\gamma = \frac{1}{\|\mathbf{C}\|_2^2}$, see Parikh and Boyd [38] for more details. The iterative process converges to the optimized sparse coefficient \mathbf{w} .

4. Experiments

We comprehensively evaluate the performance of SCoCCA across multiple experiments and under several metrics, assessing its *purity* and *editing* capabilities, *sparsity* of the concept decomposition, and *reconstruction* accuracy.

Algorithm 1 Sparse Concept CCA (SCoCCA)

Require: Paired embeddings (\mathbf{X}, \mathbf{Y}) , number of concepts k , sparsity coefficient λ , unseen embedding \mathbf{x}_0

Concept Discovery

- 1: Center embeddings: $\bar{\mathbf{X}} \leftarrow \mathbf{X} - \mathbf{1} \mu_X^\top$, $\bar{\mathbf{Y}} \leftarrow \mathbf{Y} - \mathbf{1} \mu_Y^\top$
- 2: Compute projection: $\mathbf{U} \leftarrow \sum_{\mathbf{x}}^{-1/2} \mathbf{Q}_x$ (Eq. (10))
- 3: Derive concept dictionary: $\mathbf{C} \leftarrow \sum_{\mathbf{x}} \mathbf{U}$ (Eq. (11))
- 4: Match concepts to textual attributes: solve $\mathbf{B} \in \{0, 1\}^{k \times M}$ (Eq. (14))
- 5: **Output:** Concept Bank \mathcal{C}

Concept Decomposition

- 6: Center unseen embedding: $\bar{\mathbf{x}}_0 \leftarrow \mathbf{x}_0 - \mu_X$
 - 7: Optimize sparse concept activations through Lasso: $\mathbf{w} \leftarrow \min_{\mathbf{w} \in \mathbb{R}^k} F(\mathbf{w})$ (Eq. (15))
 - 8: **Output:** Sparse coefficients \mathbf{w} and interpretable reconstruction $\hat{\mathbf{x}} = \mathbf{C}\mathbf{w} + \mu_X$
-

Implementation Details. All experiments are conducted using CLIP ViT-L/14 [41] as the backbone, while results on CLIP ViT-B/32 are provided in the Supp. Unless stated otherwise, we use a subset of 500 randomly-chosen classes from ImageNet [8] as the primary dataset, where the concept bank consists of items corresponding to ImageNet classes (e.g., ‘‘An image of a beagle’’). To perform concept matching using the Hungarian algorithm [25] we use the SciPy library. For computing coefficient vectors w , as in Eq. 15, we use the scikit-learn [39] FISTA solver. We compare our method against single-modality methods: TCAV [21], Varimax [60], NMF, K-Means, and CLIP [41]; and SpLiCE [5], a recent dual-modality approach. We use the official SpLiCE implementation provided at [6], and have implemented the other methods and baselines, following the original papers implementation details. We used the scikit-learn [39] implementation for the K-Means [33] clustering method using k as number of classes on the centered ImageNet[8] embeddings. We have used the multiplicative updates solver in scikit-learn [39] to implement the NMF [26] method. All the results are summarized in Tab. 1.

4.1. Metrics

We train a logistic regression classifier h on the ImageNet training set to predict among M classes. In all metrics we average on the entire dataset unless explicitly written otherwise.

4.1.1. Concept Purity

A key question is how well the computed concept vectors align with semantic concepts. We evaluate this through two

Table 1. **Comprehensive Performance Comparison.** Results comparing concept decomposition methods on subset of 500 random classes from ImageNet [8], grouped into dual-modality and single-modality approaches, and evaluated across a wide range of metrics. Best results are shown in **bold**, and second-best are underlined. SCoCCA achieves state-of-the-art or on-par performance in Reconstruction, as well as in Purity & Editing. Rightmost column shows CLIP zero-shot performance. Note the SCoCCA obtains CLIP-level performance in accuracy.

Category	Metric	Dual-Modality		Single-Modality				Baseline
		SCoCCA (Ours)	SpLiCE [5]	TCAV[21]	Varimax[60]	NMF	K-Means	CLIP[41]
Purity and Editing	Ablation prob. drop (\uparrow)	<u>0.87</u>	0.20	0.93	0.81	0.01	0.47	-
	Target prob gain (\uparrow)	0.95	0.36	0.10	<u>0.75</u>	0.02	-0.09	-
	Img residual cosine (\uparrow)	0.76	<u>0.70</u>	0.67	<u>0.67</u>	0.63	0.74	-
	Zero-shot accuracy (\uparrow)	0.74	0.48	0.62	<u>0.65</u>	0.12	0.53	0.75
	Zero-shot precision@5 (\uparrow)	0.85	0.61	0.59	<u>0.75</u>	0.29	0.70	0.85
Sparsity	Concepts orthogonality (\uparrow)	<u>0.93</u>	0.88	0.85	1.0	0.23	0.86	-
	Energy coverage@10 (\uparrow)	0.30	<u>0.89</u>	0.21	0.33	0.08	1.0	-
	Hoyer sparsity (\uparrow)	0.38	<u>0.88</u>	0.28	0.38	0.13	1.0	-
Reconstruction	Cosine rec. similarity (\uparrow)	0.99	0.58	0.50	<u>0.90</u>	0.74	0.84	-
	Relative L_2 rec. error (\downarrow)	0.04	0.35	0.28	<u>0.15</u>	0.43	0.29	-

scenarios: (1) *concept ablation*, where the coefficient corresponding to a specific concept is set to zero, and (2) *concept insertion*, where a concept activation value is moved into another concept entry. These modifications yield a new coefficient vector, denoted as \mathbf{w}_0^* , and its corresponding reconstruction, $\hat{\mathbf{x}}_0^*$.

Ablation probability drop. Following Fel et al. [9], we evaluate how well a concept vector \mathbf{c}_i captures its associated class by ablating the i -th entry in \mathbf{w}_0 and then classifying the reconstructed sample $\hat{\mathbf{x}}_0^*$ using the trained classifier h . The metric is defined as:

$$[h(\mathbf{x}_0)]_i - [h(\hat{\mathbf{x}}_0^*)]_i. \quad (18)$$

We report the average over the entire test-set of ImageNet-500.

Target probability gain. Additionally, we analyze the insertion case. For a source concept \mathbf{c}_i , and a target concept \mathbf{c}_j , we edit \mathbf{w}_0 by transferring the weight of the i -th entry to the j -th entry, leaving the i -th entry zeroed. Then the metric is defined as:

$$[h(\hat{\mathbf{x}}_0^*)]_j - [h(\mathbf{x}_0)]_j \quad (19)$$

We randomly select $\approx 15\%$ of the classes in the dataset, and compute the average over all their possible combinations.

Image residual cosine. While the aforementioned metrics evaluate how well the coefficient vector captures individual concepts through ablation and insertion, they overlook how these operations affect the remaining concepts. In the insertion case, to eliminate the impact of concept i from

x_0 and j from \hat{x}_0^* , we first compute their residuals with respect to the corresponding concept means:

$$\mathbf{r}_i(\mathbf{x}_0) = \mathbf{x}_0 - \mathbf{P}_{\mu_i}(\mathbf{x}_0), \quad \mathbf{r}_j(\hat{\mathbf{x}}_0^*) = \hat{\mathbf{x}}_0^* - \mathbf{P}_{\mu_j}(\hat{\mathbf{x}}_0^*),$$

where μ_i and μ_j denote the unit-norm mean embeddings of classes i and j , respectively, and $\mathbf{P}_{\mu}(\mathbf{x})$ is the projection of \mathbf{x} onto vector μ . The residual cosine similarity is then defined as:

$$\frac{\langle \mathbf{r}_i(\mathbf{x}_0), \mathbf{r}_j(\hat{\mathbf{x}}_0^*) \rangle}{\|\mathbf{r}_i(\mathbf{x}_0)\|_2 \|\mathbf{r}_j(\hat{\mathbf{x}}_0^*)\|_2} \quad (20)$$

Similar to the target probability gain metric, we randomly select $\approx 15\%$ of the classes in the dataset, and compute the average over all their possible combinations.

4.1.2. Sparsity

Concept orthogonality. The orthogonality metric is defined as:

$$1 - \mathbb{E}_{i \neq j} \left[\left\| \frac{\mathbf{c}_i^\top \mathbf{c}_j}{\|\mathbf{c}_i\|_2 \|\mathbf{c}_j\|_2} \right\| \right] \quad (21)$$

It equals 1 when the concepts are mutually orthogonal and approaches 0 when concepts are collinear.

Hoyer sparsity. The Hoyer index [16] is

$$\frac{\sqrt{k} - \|\mathbf{w}\|_1 / \|\mathbf{w}\|_2}{\sqrt{k} - 1}, \quad (22)$$

where k is the dimension of \mathbf{w} . The overall score is the average of the entire test-set. This scale-invariant index equals 0 for a constant vector and approaches 1 when all mass concentrates on a single concept. It captures how concentrated the weight distribution is without relying on a hard threshold.



Figure 3. **Concept Retrieval Generalization.** Retrieval of the top four MSCOCO [32] images with the highest activation for the concepts *Microwave* and *Traffic Light*, where the concept bank was calibrated on ImageNet only (images are shown in descending order). While SCoCCA retrieves images with a clear presence of the concept, other methods in some cases return images with little or no evidence of the desired concept.

Energy coverage @10. For concept coefficients \mathbf{w}_i we measure how much of the total energy is explained by the 10 most contributing concepts by:

$$\frac{1}{n} \sum_{i=1}^n \frac{\sum_{j \in \text{top-10}} (\mathbf{w}_i)_j^2 \|\hat{\mathbf{c}}_j\|_2^2}{\sum_{j=1}^k (\mathbf{w}_i)_j^2 \|\hat{\mathbf{c}}_j\|_2^2}, \quad (23)$$

where $\hat{\mathbf{c}} = \mathbf{c} / \|\mathbf{c}\|_2$. Higher values of this metric indicate that a small number of concepts account for most of the reconstruction energy.

4.1.3. Reconstruction

Relative ℓ_2 reconstruction error. This metric quantifies the scale-normalized discrepancy between original and reconstructed embeddings:

$$\frac{1}{n} \sum_{i=1}^n \frac{\|\mathbf{x}_i - \hat{\mathbf{x}}_i\|_2^2}{\|\mathbf{x}_i\|_2^2}. \quad (24)$$

It measures the fraction of signal energy not captured by the reconstruction, providing a scale-invariant complement to the cosine similarity, which focuses on angular alignment.

Cosine reconstruction similarity. This metric quantifies the directional consistency between original and reconstructed embeddings:

$$\frac{1}{n} \sum_{i=1}^n \frac{\langle \mathbf{x}_i, \hat{\mathbf{x}}_i \rangle}{\|\mathbf{x}_i\|_2 \|\hat{\mathbf{x}}_i\|_2} \quad (25)$$

It captures alignment in direction, which is essential for similarity-based retrieval and zero-shot classification methods that rely on normalized embeddings.

4.2. Results analysis

The quantitative results across *Purity*, *Editing*, *Sparsity*, and *Reconstruction* metrics are summarized in Tab. 1. SCoCCA consistently outperforms competing approaches, achieving top or comparable performance in nearly all metrics. Its advantages are particularly pronounced in purity, editing, and reconstruction, where the improvements over prior dual- and single-modality methods are substantial rather than marginal, highlighting the effectiveness of SCoCCA’s concept decomposition in preserving semantics while enabling precise control. Note that SCoCCA obtains CLIP-level performance on accuracy.

Purity and concept editing. SCoCCA consistently outperforms all baselines across purity-related metrics. It achieves the highest residual cosine similarity (0.76), indicating that reconstructed embeddings preserve fine-grained semantic structure without over-smoothing. The method also attains a substantial target probability gain (0.95), showing that amplifying a discovered concept reliably strengthens its associated class prediction, and a strong source probability drop (0.87). Together, these results demonstrate that SCoCCA achieves high semantic purity while providing precise and disentangled control over concept activations, surpassing both multimodal and single-modality baselines.

Sparsity. K-Means inherently produces one-hot concept assignments, yielding perfect ℓ_0 sparsity by definition. Similarly, Varimax [60] yields orthogonal concept vectors by construction, resulting in ideal scores on the orthogonality metric. While SCoCCA achieves lower orthogonality

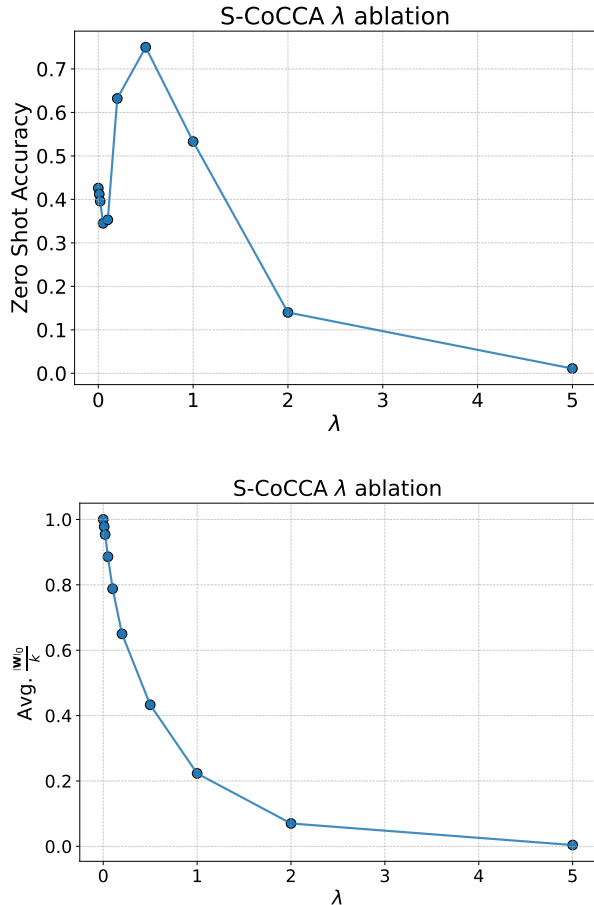


Figure 4. λ ablation for SCoCCA on ImageNet-500.

Top: Zero-shot accuracy on ImageNet-500 as a function the λ used when solving the sparse CoCCA coding objective in (15). **Bottom:** $\|w\|_0$ normalized by k , as function of λ . In both plots, $\lambda = 0$ corresponds to the CoCCA baseline without the sparsity penalty. The curves shows that forcing sparsity yields substantially higher zero-shot accuracy than the non-sparse baseline.

and sparsity values, incorporating sparsity regularization increases the sparsity of the learned weights, as illustrated in Figure 4 (bottom).

Reconstruction. SCoCCA achieves near-perfect reconstruction fidelity, attaining the highest cosine reconstruction similarity (0.99) and the lowest relative ℓ_2 error (0.02), indicating that its decomposed representations can almost perfectly recover the original embeddings while maintaining their directional structure. Furthermore, it attains strong zero-shot accuracy (0.74) and precision@5 (0.85), on par with or surpassing the CLIP baseline, demonstrating that reconstruction quality directly translates to preserved discriminative performance. These results confirm that SCoCCA’s concept decomposition preserves both geometric integrity

and semantic predictiveness of the underlying multimodal space.

Generalization. Generalization is a key property of interpretable concept models, as meaningful concepts should extend beyond the dataset on which they were discovered. By leveraging both the image and text representations of CLIP, SCoCCA benefits from the unified multimodal embedding space of a foundation model, which inherently promotes generalization. To evaluate this, we apply SCoCCA’s concept dictionary, calibrated on ImageNet, to the MSCOCO [32] validation set and perform a retrieval experiment using a concept query (e.g., *microwave*) to retrieve the top-4 images with the highest concept activations. Two qualitative examples are shown in Fig. 3, with additional results provided in the Supp. SCoCCA consistently retrieves images that accurately depict the target concept, whereas competing methods often return images where the concept appears only vaguely or is absent. For instance, in the *microwave* query, both SpLiCE and Varimax retrieve images of an entire kitchen, and in the *Traffic Light* query, retrieved images often show general roads or stop signs, sometimes containing only the environment without the concept itself.

4.3. Ablation Study

Fig. 4 demonstrates the zero-shot accuracy as a function of the average fraction of active concepts on ImageNet-500, obtained by varying the sparsity coefficient λ , which balances the sparsity and reconstruction terms in Eq. 15. This measure reflects the relative number of non-zero elements in the weight vector w , indicating the degree of sparsity. As λ increases, sparsity grows accordingly, leading to fewer active concepts. The best performance is achieved when roughly half of the concept weights are zeroed out, suggesting that moderate sparsity yields the most discriminative representations. The ablation plot also includes the case of $\lambda = 0$, which corresponds to the CoCCA baseline where no sparsity is enforced.

5. Conclusion

We introduce SCoCCA, a method that bridges cross-modal alignment with concept-based explainability. Built upon Canonical Correlation Analysis (CCA), SCoCCA discovers a shared latent subspace between image and text embeddings while enforcing sparsity for interpretability. Unlike existing concept-based models that rely only on a single modality, SCoCCA aligns multimodal concepts, deriving Concept Activation Vectors (CAVs) that correspond to meaningful semantic directions shared across modalities. By leveraging the CCA objective, SCoCCA implicitly enhances the alignment term of the InfoNCE loss, providing a training-free mechanism to refine pretrained representations

such as CLIP. Through extensive experiments, we show that this approach not only enables precise concept decomposition and manipulation but also achieves state-of-the-art performance in reconstruction, as well as in purity and editing metrics, demonstrating that SCoCCA produces both faithful and highly controllable concept representations. Moreover, the learned multimodal concept space generalizes beyond the data used for discovery, supporting retrieval and editing on out-of-distribution images. Taken together, these results indicate that SCoCCA offers a simple and principled way to expose and control the internal conceptual structure of vision-language models, as required for transparent and reliable deployment.

References

- [1] Julia Amann, Alessandro Blasimme, Effy Vayena, Dietmar Frey, Vince I Madai, and Precise4Q Consortium. Explainability for artificial intelligence in healthcare: a multidisciplinary perspective. *BMC medical informatics and decision making*, 20(1):310, 2020. 1
- [2] Galen Andrew, Raman Arora, Jeff Bilmes, and Karen Livescu. Deep canonical correlation analysis. In *International conference on machine learning*, pages 1247–1255. PMLR, 2013. 3
- [3] Amir Beck and Marc Teboulle. A fast iterative shrinkage-thresholding algorithm for linear inverse problems. *SIAM Journal on Imaging Sciences*, 2(1):183–202, 2009. 5
- [4] Roy Betsler, Meir Yossef Levi, and Guy Gilboa. Whited clip as a likelihood surrogate of images and captions. In *Proceedings of the 42nd International Conference on Machine Learning*, Vancouver, Canada, 2025. PMLR. 2, 3
- [5] Usha Bhalla, Alex Oesterling, Suraj Srinivas, Flavio Calmon, and Himabindu Lakkaraju. Interpreting clip with sparse linear concept embeddings (splice). *Advances in Neural Information Processing Systems*, 37:84298–84328, 2024. 2, 3, 5, 6, 1
- [6] Usha Bhalla, Alex Oesterling, S. Srinivas, Fernando P. Calmon, and Himabindu Lakkaraju. Splice: Sparse linear concept embeddings. GitHub repository, 2025. Available at <https://github.com/AI4LIFE-GROUP/SpLiCE/tree/main>. 5
- [7] Kushal Chauhan, Rishabh Tiwari, Jan Freyberg, Pradeep Shenoy, and D. Dvijotham. Interactive concept bottleneck models. In *Proceedings of the AAAI Conference on Artificial Intelligence (AAAI)*, 2023. 1, 3
- [8] Jia Deng, Wei Dong, Richard Socher, Li-Jia Li, Kai Li, and Li Fei-Fei. Imagenet: A large-scale hierarchical image database. In *2009 IEEE conference on computer vision and pattern recognition*, pages 248–255. Ieee, 2009. 5, 6, 1
- [9] Thomas Fel, Victor Boutin, Louis Béthune, Rémi Cadène, Mazda Moayeri, Léo Andéol, Mathieu Chalvidal, and Thomas Serre. A holistic approach to unifying automatic concept extraction and concept importance estimation. *Advances in Neural Information Processing Systems*, 36:54805–54818, 2023. 3, 6
- [10] Thomas Fel, Agustin Picard, Louis Bethune, Thibaut Boissin, David Vigouroux, Julien Colin, Rémi Cadène, and Thomas Serre. Craft: Concept recursive activation factorization for explainability. In *Proceedings of the IEEE/CVF Conference on Computer Vision and Pattern Recognition*, pages 2711–2721, 2023. 2
- [11] Thomas Fel, Ekdeep Singh Lubana, Jacob S Prince, Matthew Kowal, Victor Boutin, Isabel Papadimitriou, Binxu Wang, Martin Wattenberg, Demba Ba, and Talia Konkle. Archetypal sae: Adaptive and stable dictionary learning for concept extraction in large vision models. *arXiv preprint arXiv:2502.12892*, 2025. 2
- [12] Amirata Ghorbani, James Wexler, James Y Zou, and Been Kim. Towards automatic concept-based explanations. *Advances in neural information processing systems*, 32, 2019. 2

- [13] Souhail Hadgi, Luca Moschella, Andrea Santilli, Diego Gomez, Qixing Huang, Emanuele Rodolà, Simone Melzi, and Maks Ovsjanikov. Escaping plato’s cave: Towards the alignment of 3d and text latent spaces. In *Proceedings of the IEEE/CVF Conference on Computer Vision and Pattern Recognition (CVPR)*, pages 19825–19835, 2025. 2
- [14] Harold Hotelling. Relations between two sets of variates. *Biometrika*, 28(3/4):321–377, 1936. 3
- [15] Harold Hotelling. Relations between two sets of variates. In *Breakthroughs in statistics: methodology and distribution*, pages 162–190. Springer, 1992. 2
- [16] Patrik O Hoyer. Non-negative matrix factorization with sparseness constraints. *Journal of machine learning research*, 5(Nov):1457–1469, 2004. 6
- [17] Takoua Jendoubi and Korbinian Strimmer. A whitening approach to probabilistic canonical correlation analysis for omics data integration. *BMC bioinformatics*, 20(1):15, 2019. 4
- [18] Sonia Joseph, Praneet Suresh, Ethan Goldfarb, Lorenz Hufe, Yossi Gandelsman, Robert Graham, Danilo Bzdok, Wojciech Samek, and Blake Aaron Richards. Steering clip’s vision transformer with sparse autoencoders. *arXiv preprint arXiv:2504.08729*, 2025. 2
- [19] Henry F Kaiser. The varimax criterion for analytic rotation in factor analysis. *Psychometrika*, 23(3):187–200, 1958. 3, 2
- [20] Agnan Kessy, Alex Lewin, and Korbinian Strimmer. Optimal whitening and decorrelation. *The American Statistician*, 72(4):309–314, 2018. 3
- [21] Been Kim, Martin Wattenberg, Justin Gilmer, Carrie Cai, James Wexler, Fernanda Viégas, and Rory Sayres. Interpretability beyond feature attribution: Quantitative testing with concept activation vectors. In *Proceedings of the 35th International Conference on Machine Learning (ICML)*, 2018. 1, 2, 3, 5, 6
- [22] Eunji Kim, Dahuin Jung, Sangha Park, Siwon Kim, and Sungho Yoon. Probabilistic concept bottleneck models. *arXiv preprint arXiv:2306.01574*, 2023. 1
- [23] Pang Wei Koh, Thao Nguyen, Yew Siang Tang, Stephen Mussmann, Emma Pierson, Been Kim, and Percy Liang. Concept bottleneck models. In *Proceedings of the 37th International Conference on Machine Learning (ICML)*, 2020. 3
- [24] Pang Wei Koh, Thao Nguyen, Yew Siang Tang, Stephen Mussmann, Emma Pierson, Been Kim, and Percy Liang. Concept bottleneck models. In *Proceedings of the 37th International Conference on Machine Learning*, pages 5338–5348. PMLR, 2020. 1
- [25] Harold W. Kuhn. The Hungarian method for the assignment problem. *Naval Research Logistics Quarterly*, 2(1-2):83–97, 1955. 5
- [26] Daniel Lee and H Sebastian Seung. Algorithms for non-negative matrix factorization. *Advances in neural information processing systems*, 13, 2000. 5, 3
- [27] Sharon Lee, Yunzhi Zhang, Shangzhe Wu, and Jiajun Wu. Language-informed visual concept learning. *arXiv preprint arXiv:2312.03587*, 2023. 3
- [28] Meir Yossef Levi and Guy Gilboa. The double ellipsoid geometry of clip. In *Proceedings of the 42nd International Conference on Machine Learning*, Vancouver, Canada, 2025. PMLR. 2, 3
- [29] Jiaang Li, Yova Kementchedjheva, Constanza Fierro, and Anders Søgaard. Do vision and language models share concepts? a vector space alignment study. *Transactions of the Association for Computational Linguistics*, 12:1232–1249, 2024. 3
- [30] Victor Weixin Liang, Yuhui Zhang, Yongchan Kwon, Serena Yeung, and James Y Zou. Mind the gap: Understanding the modality gap in multi-modal contrastive representation learning. In *Advances in Neural Information Processing Systems*, pages 17612–17625. Curran Associates, Inc., 2022. 2, 3
- [31] Hyesu Lim, Jinho Choi, Jaegul Choo, and Steffen Schneider. Sparse autoencoders reveal selective remapping of visual concepts during adaptation. *arXiv preprint arXiv:2412.05276*, 2024. 2
- [32] Tsung-Yi Lin, Michael Maire, Serge Belongie, James Hays, Pietro Perona, Deva Ramanan, Piotr Dollár, and C Lawrence Zitnick. Microsoft coco: Common objects in context. In *European conference on computer vision*, pages 740–755. Springer, 2014. 7, 8
- [33] Stuart Lloyd. Least squares quantization in pcm. *IEEE transactions on information theory*, 28(2):129–137, 1982. 5, 3
- [34] Julien Mairal, Francis Bach, Jean Ponce, et al. Sparse modeling for image and vision processing. *Foundations and Trends® in Computer Graphics and Vision*, 8(2-3):85–283, 2014. 3
- [35] Leon Mirsky. A trace inequality of john von neumann. *Monatshefte für mathematik*, 79(4):303–306, 1975. 2
- [36] Mazda Moayeri, Keivan Rezaei, Maziar Sanjabi, and Soheil Feizi. Text2concept: Concept activation vectors directly from text. In *Proceedings of the IEEE/CVF Conference on Computer Vision and Pattern Recognition*, pages 3744–3749, 2023. 1
- [37] Aaron van den Oord, Yazhe Li, and Oriol Vinyals. Representation learning with contrastive predictive coding. *arXiv preprint arXiv:1807.03748*, 2018. 2
- [38] Neal Parikh and Stephen Boyd. Proximal algorithms. *Foundations and Trends in Optimization*, 1(3):127–239, 2014. 5
- [39] Fabian Pedregosa, Gaël Varoquaux, Alexandre Gramfort, Vincent Michel, Bertrand Thirion, Olivier Grisel, Mathieu Blondel, Peter Prettenhofer, Ron Weiss, Vincent Dubourg, et al. Scikit-learn: Machine learning in python. *the Journal of machine Learning research*, 12:2825–2830, 2011. 5
- [40] Jacob Pfau, Albert T Young, Jerome Wei, Maria L Wei, and Michael J Keiser. Robust semantic interpretability: Revisiting concept activation vectors. *arXiv preprint arXiv:2104.02768*, 2021. 1
- [41] Alec Radford, Jong Wook Kim, Chris Hallacy, Aditya Ramesh, Gabriel Goh, Sandhini Agarwal, Girish Sastry, Amanda Askell, Pamela Mishkin, Jack Clark, et al. Learning transferable visual models from natural language supervision. In *International conference on machine learning*, pages 8748–8763. Pmlr, 2021. 2, 5, 6, 1

- [42] Aditya Ramesh, Prafulla Dhariwal, Alex Nichol, Casey Chu, and Mark Chen. Hierarchical text-conditional image generation with clip latents. *arXiv preprint arXiv:2204.06125*, 1(2):3, 2022. 4
- [43] Yoshihide Sawada and Keigo Nakamura. Concept bottleneck model with additional unsupervised concepts. *IEEE Access*, 10:41758–41765, 2022. 3
- [44] Simon Schrodi, David T Hoffmann, Max Argus, Volker Fischer, and Thomas Brox. Two effects, one trigger: On the modality gap, object bias, and information imbalance in contrastive vision-language representation learning. *arXiv preprint arXiv:2404.07983*, 2024. 3
- [45] Christoph Schuhmann, Richard Vencu, Romain Beaumont, Robert Kaczmarczyk, Clayton Mullis, Aarush Katta, Theo Coombes, Jenia Jitsev, and Aran Komatsuzaki. Laion-400m: Open dataset of clip-filtered 400 million image-text pairs. *arXiv preprint arXiv:2111.02114*, 2021. 2
- [46] Sungbin Shin, Yohan Jo, Sungsoo Ahn, and Namhoon Lee. A closer look at the intervention procedure of concept bottleneck models. In *International Conference on Machine Learning*, pages 31504–31520. PMLR, 2023. 3
- [47] David Steinmann, Wolfgang Stammer, Felix Friedrich, and Kristian Kersting. Learning to intervene on concept bottlenecks. *arXiv preprint arXiv:2308.13453*, 2023. 3
- [48] Samuel Stevens, Wei-Lun Chao, Tanya Berger-Wolf, and Yu Su. Sparse autoencoders for scientifically rigorous interpretation of vision models. *arXiv preprint arXiv:2502.06755*, 2025. 2
- [49] Chung-En Sun, Tuomas Oikarinen, Berk Ustun, and Tsui-Wei Weng. Concept bottleneck large language models. *arXiv preprint arXiv:2412.07992*, 2024. 3
- [50] Zhongkai Sun, Prathusha K Sarma, William Sethares, and Erik P Bucy. Multi-modal sentiment analysis using deep canonical correlation analysis. *arXiv preprint arXiv:1907.08696*, 2019. 2
- [51] Robert Tibshirani. Regression shrinkage and selection via the lasso. *Journal of the Royal Statistical Society: Series B*, 58(1):267–288, 1996. 4, 5
- [52] Moritz Vandenhirtz, Sonia Laguna, Ričards Marcinkevičs, and Julia E. Vogt. Stochastic concept bottleneck models. In *Proceedings of the 38th Conference on Neural Information Processing Systems (NeurIPS)*, 2024. 3
- [53] Tongzhou Wang and Phillip Isola. Understanding contrastive representation learning through alignment and uniformity on the hypersphere. In *International conference on machine learning*, pages 9929–9939. PMLR, 2020. 4
- [54] Daniela M Witten, Robert Tibshirani, and Trevor Hastie. A penalized matrix decomposition, with applications to sparse principal components and canonical correlation analysis. *Biostatistics*, 10(3):515–534, 2009. 3
- [55] Amitai Yacobi, Nir Ben-Ari, Ronen Talmon, and Uri Shalem. Learning shared representations from unpaired data. *arXiv preprint arXiv:2505.21524*, 2025. 2
- [56] Mert Yuksekgonul, Maggie Wang, and James Zou. Post-hoc concept bottleneck models. *arXiv preprint arXiv:2205.15480*, 2022. 1
- [57] Éloi Zablocki, Hédi Ben-Younes, Patrick Pérez, and Matthieu Cord. Explainability of deep vision-based autonomous driving systems: Review and challenges. *International Journal of Computer Vision*, 130(10):2425–2452, 2022. 1
- [58] Yuan Zang, Tian Yun, Hao Tan, Trung Bui, and Chen Sun. Pre-trained vision-language models learn discoverable visual concepts. *arXiv preprint arXiv:2404.12652*, 2024. 3
- [59] Ruihan Zhang, Prashan Madumal, Tim Miller, Krista A Ehinger, and Benjamin IP Rubinstein. Invertible concept-based explanations for cnn models with non-negative concept activation vectors. In *Proceedings of the AAAI Conference on Artificial Intelligence*, pages 11682–11690, 2021. 1, 2
- [60] Jitian Zhao, Chenghui Li, Frederic Sala, and Karl Rohe. Quantifying structure in clip embeddings: A statistical framework for concept interpretation. *arXiv preprint arXiv:2506.13831*, 2025. 1, 3, 5, 6, 7, 2

SCoCCA: Multi-modal Sparse Concept Decomposition via Canonical Correlation Analysis

Supplementary Material

6. Ablation of k hyperparameter

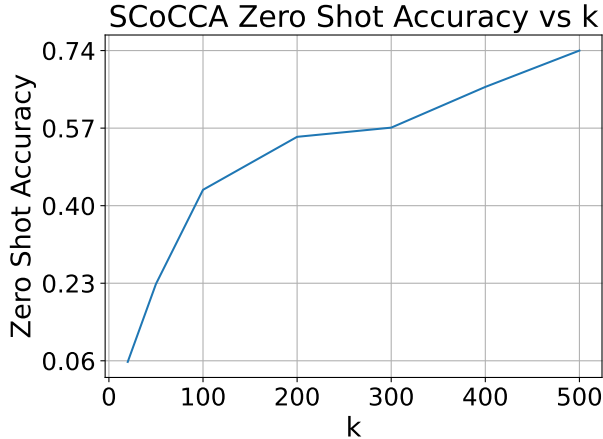


Figure 5. **ablation of k hyperparameter** Zero-Shot Accuracy performance on test set of ImageNet-500, as a function of k , the number of concepts computed, for the SCoCCA method. As more concepts allows better separation, this is a monotone increasing function. However the rate of steepness decreases, as additional concepts yield less of a return in classification.

7. Comparison on CLIP B-32 model

Table 2. **Comprehensive Performance Comparison.** Results comparing concept decomposition methods on subset of 500 random classes from ImageNet [8], similar to Table 1, but for **CLIP model B-32**. Best results are shown in **bold**, and second-best are underlined. We observe similar trends like Table 1. As expected from a smaller model, for same number of $k = 500$, reconstruction metrics improve, whereas Purity metrics decrease.

Category	Metric	Dual-Modality		Single-Modality				Baseline
		SCoCCA (Ours)	SpLiCE [5]	TCAV[21]	Varimax[60]	NMF	K-Means	CLIP[41]
Purity and Editing	Ablation prob. drop (\uparrow)	<u>0.77</u>	0.12	0.79	0.73	0.00	0.37	-
	Target prob gain (\uparrow)	0.72	0.11	0.02	<u>0.61</u>	-0.19	-0.39	-
	Img residual cosine (\uparrow)	0.70	<u>0.63</u>	0.58	0.57	0.49	0.68	-
	Zero-shot accuracy (\uparrow)	0.60	0.37	0.48	<u>0.52</u>	0.10	0.40	0.63
	Zero-shot precision@5 (\uparrow)	0.81	0.58	0.71	<u>0.74</u>	0.25	0.68	0.82
Sparsity	Concepts orthogonality (\uparrow)	<u>0.92</u>	<u>0.92</u>	0.81	1.0	0.23	0.83	-
	Energy coverage@10 (\uparrow)	0.38	<u>0.79</u>	0.44	0.51	0.07	1.0	-
	Hoyer sparsity (\uparrow)	0.58	<u>0.90</u>	0.39	0.41	0.14	1.0	-
Reconstruction	Cosine rec. similarity (\uparrow)	1.00	0.69	0.64	1.00	0.84	<u>0.92</u>	-
	Relative L_2 rec. error (\downarrow)	0.00	0.22	0.11	<u>0.02</u>	0.40	0.27	-

8. Derivation of CCA via whitening and SVD

8.1. Setup

Let $\mathbf{X}, \mathbf{Y} \in \mathbb{R}^{n \times d}$ denote paired samples, with rows centered to have zero empirical mean. Define empirical covariance and cross-covariance matrices:

$$\Sigma_X := \frac{1}{n} \mathbf{X}^\top \mathbf{X} \in \mathbb{R}^{d \times d}, \quad \Sigma_Y := \frac{1}{n} \mathbf{Y}^\top \mathbf{Y} \in \mathbb{R}^{d \times d}, \quad (26)$$

and

$$\Sigma_{XY} := \frac{1}{n} \mathbf{X}^\top \mathbf{Y} \in \mathbb{R}^{d \times d}. \quad (27)$$

Assume Σ_X and Σ_Y are symmetric positive definite, so that their symmetric inverse square roots $\Sigma_X^{-1/2}$ and $\Sigma_Y^{-1/2}$ are well defined.

Canonical Correlation Analysis (CCA) with target dimension k solves

$$\max_{\mathbf{U}, \mathbf{V} \in \mathbb{R}^{d \times k}} \text{tr} [\mathbf{U}^\top \Sigma_{XY} \mathbf{V}] \quad (28)$$

subject to the normalization constraints

$$\mathbf{U}^\top \Sigma_X \mathbf{U} = \mathbf{I}_k, \quad \mathbf{V}^\top \Sigma_Y \mathbf{V} = \mathbf{I}_k. \quad (29)$$

8.2. Whitening and reduction to an orthogonal problem

Introduce the change of variables

$$\mathbf{A} := \Sigma_X^{-1/2} \mathbf{U}, \quad \mathbf{B} := \Sigma_Y^{-1/2} \mathbf{V}, \quad (30)$$

so that

$$\mathbf{U} = \Sigma_X^{-1/2} \mathbf{A}, \quad \mathbf{V} = \Sigma_Y^{-1/2} \mathbf{B}. \quad (31)$$

The constraints (29) become

$$\mathbf{A}^\top \mathbf{A} = \mathbf{U}^\top \Sigma_X \mathbf{U} = \mathbf{I}_k, \quad \mathbf{B}^\top \mathbf{B} = \mathbf{V}^\top \Sigma_Y \mathbf{V} = \mathbf{I}_k.$$

Thus \mathbf{A} and \mathbf{B} have orthonormal columns.

Define the whitened cross-covariance matrix

$$\mathbf{M} := \Sigma_X^{-1/2} \Sigma_{XY} \Sigma_Y^{-1/2} \in \mathbb{R}^{d \times d}. \quad (32)$$

Using (31), the CCA objective (28) can be written as

$$\text{tr} [\mathbf{U}^\top \Sigma_{XY} \mathbf{V}] = \text{tr} [\mathbf{A}^\top \Sigma_X^{-1/2} \Sigma_{XY} \Sigma_Y^{-1/2} \mathbf{B}] \quad (33)$$

$$= \text{tr} [\mathbf{A}^\top \mathbf{M} \mathbf{B}]. \quad (34)$$

Hence CCA is equivalent to the orthogonal trace maximization

$$\max_{\mathbf{A}, \mathbf{B} \in \mathbb{R}^{d \times k}} \text{tr} [\mathbf{A}^\top \mathbf{M} \mathbf{B}] \quad (35)$$

subject to

$$\mathbf{A}^\top \mathbf{A} = \mathbf{I}_k, \quad \mathbf{B}^\top \mathbf{B} = \mathbf{I}_k. \quad (36)$$

SVD of \mathbf{M} and closed form for \mathbf{U}, \mathbf{V}

Compute the singular value decomposition of \mathbf{M} :

$$\mathbf{M} = \mathbf{Q}_X \mathbf{S} \mathbf{Q}_Y^\top, \quad (37)$$

where

- $\mathbf{Q}_X, \mathbf{Q}_Y \in \mathbb{R}^{d \times d}$ are orthogonal, $\mathbf{Q}_X^\top \mathbf{Q}_X = \mathbf{Q}_Y^\top \mathbf{Q}_Y = \mathbf{I}_d$,
- $\mathbf{S} = \text{diag}(s_1, \dots, s_d)$ with singular values

$$s_1 \geq s_2 \geq \dots \geq s_d \geq 0. \quad (38)$$

Let $\mathbf{Q}_{X,k} \in \mathbb{R}^{d \times k}$ and $\mathbf{Q}_{Y,k} \in \mathbb{R}^{d \times k}$ denote the matrices formed by the first k columns of \mathbf{Q}_X and \mathbf{Q}_Y respectively, and let

$$\mathbf{S}_k := \text{diag}(s_1, \dots, s_k) \in \mathbb{R}^{k \times k}.$$

A standard result (von Neumann's trace inequality [35]) implies that the solution of (35) is obtained by taking

$$\mathbf{A}^* = \mathbf{Q}_{X,k}, \quad \mathbf{B}^* = \mathbf{Q}_{Y,k}, \quad (39)$$

up to a common right multiplication by an orthogonal matrix in $\mathbb{R}^{k \times k}$. For this choice,

$$\text{tr} [(\mathbf{A}^*)^\top \mathbf{M} \mathbf{B}^*] = \text{tr}(\mathbf{S}_k) = \sum_{i=1}^k s_i, \quad (40)$$

which is the maximum possible value of (35).

Back-substituting (39) into (31), we obtain the CCA projection matrices in closed form:

$$\mathbf{U}^* = \Sigma_X^{-1/2} \mathbf{Q}_{X,k}, \quad \mathbf{V}^* = \Sigma_Y^{-1/2} \mathbf{Q}_{Y,k}. \quad (41)$$

9. Methods

Varimax In a recent application by Zhao et al. [60], Varimax seeks an orthogonal rotation that concentrates loadings for interpretability. The method uses a k -truncated PCA to decompose centered image embeddings \mathbf{X} into $(\mathbf{U}_k \mathbf{D}_k) \mathbf{V}_k^\top$. It then computes an orthogonal rotation \mathbf{R} that maximizes the Varimax objective [19]. From these the authors compute a concept bank $\mathbf{C} = \mathbf{V}_k \mathbf{R}$ and coefficients $\mathbf{W} = (\mathbf{U}_k \mathbf{D}_k) \mathbf{R}$.

SpLiCE [5] sets a concept dictionary \mathbf{C} as the CLIP text embeddings of a vocabulary constructed from the 15000 most frequent one- and two-word bigrams in the text captions of the LAION-400m dataset [45]. In addition, for each dataset, the names of the classes of that dataset are added to the vocabulary, as described in the paper. Using the concept dictionary \mathbf{C} , SpLiCE decomposes an image x by solving the LASSO equation given by (15). By varying λ , different sparsity-reconstruction tradeoffs can be achieved.

K-Means For this (baseline) method, We compute the k -means [33] over the centered image embeddings \mathbf{X} . The vectors to the computed centroids are used as the concept vectors. For a new image embedding \mathbf{x}_0 , the coefficient \mathbf{w}_0 is the one-hot vector pointing to the nearest centroid.

NMF We use Nonnegative Matrix Factorization. As common, we shift \mathbf{X} to be non-negative, by computing a scalar shift $s = \min(0, \min_{i,j}(\mathbf{X}_{ij}))$, so $s \leq 0$, and then shifting $\mathbf{X}_{sh} = \mathbf{X} - s\mathbf{1}\mathbf{1}^\top$ so $\mathbf{X}_{sh} \geq 0$ entry-wise. We then solve the optimization problem

$$\min_{\mathbf{w} \geq 0, \mathbf{C} \geq 0} \frac{1}{2} \|\mathbf{X}_{sh}^T - \mathbf{C}\mathbf{W}\|_F^2 \quad (42)$$

using the multiplicative-updates (MU) solver of sklearn [26]. For reconstruction, we un-shift by adding s back.

TCAV [21] works in a supervised setting. Let f be a model providing activations from images. For a concept c , the user provides images P_c that represent that concept (e.g. “striped”) and a negative set N of random images. A binary linear classifier is trained to separate activations of the positive set $\{f(\mathbf{x}) \mid \mathbf{x} \in P_c\}$ from activations of the negative set $\{f(\mathbf{x}) \mid \mathbf{x} \in N\}$. The normal to the hyperplane separating the activations is used as that Concept Activation Vector (CAV) for concept c . For k classes we compute $\mathbf{C} \in \mathbb{R}^{d \times k}$. For comparison, coefficients \mathbf{W} are computed by solving the LASSO equation (15).